APME — Actualităţi şi Perspective în Domeniul Maşinilor Electrice
Electric Machines, Materials and Drives – Present and Trends
18, *1*, pp. 80–88, 2022

SIMULATION OF ELECTRO-THERMAL CONDITION IN A FAULTY LOW-CURRENT CONTACT

Gideon Gwanzuwang DANKAT[1] and
Laurentiu Marius DUMITRAN[1],
[1]University *Politehnica* of Bucharest, Laboratory of Electrical Materials
gdankat@elmat.pub.ro[1], dumitran@elmat.pub.ro[1]

Abstract. It has been suggested in earlier literature that the accuracy of the thermal simulation of electrical connectors is closely related to contact resistance. Contact resistance in electrical connectors occurs due to both constriction resistance (caused by narrow paths in which the current flows through the electrical connector) and film resistance (oxidized metals caused by the high resistivity of materials and impurities from the atmosphere etc.). This paper reviews the oxidation and wear affecting electrical connectors by proposing a thermal-electrical coupled finite element simulation (FEM) of the contact temperature rise of a simple contact model in COMSOL Multiphysics.

1. INTRODUCTION

Electric connectors are essential in transferring electrical signals in electrical systems and circuits. With more emphasis on global warming and environmental pollution, the automotive industries are shifting their focus to electrical vehicles. This means the number of connectors, wire harnesses, and computerized control systems will increase. There are thousands of electrical connectors in the electrical system of combustible automobiles. The reliability of these electrical connectors under harsh conditions for an extended period is very important to ensure the drivability of automobiles and the safety of lives. Previous studies have shown that contact resistance depends on the bulk material properties (mechanical and electrical), the contact's surface profile, a-spot's dimensions, and other dynamic factors [1,2]. In normal operating conditions for a given electrical contact, the resistance across the interface decreases as the applied contact load increases. This results from the surfaces of the contact needing to be more perfectly smooth. Ideally, contact between two conductors happens at numerous small areas of the apparent contact area (Fig. 1). As the current passes through these small contact areas, it gives rise to constriction resistance which can eventually cause a cut in the transmission of signal or loss of power to any electrical system through Joule heating [3]. Oxidation, mechanical wear, and harsh atmospheric conditions (dust, temperature, moisture, etc.) contribute to a higher contact resistance value degrading electrical connectors.

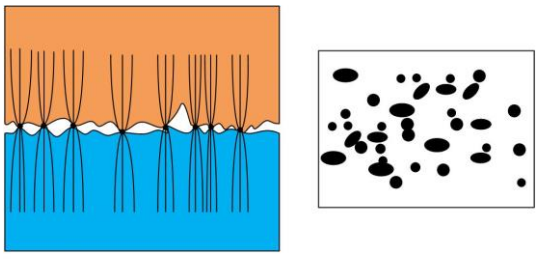

Fig. 1 – Diagram of a bulk electrical interface showing: (a) the constriction of the current lines, (b) the contact spots. [4]

ISSN / ISSN-L: 1843-5912
https://www.doi.org/10.36801/apme.2022.1.10

1.1 Contact resistance estimation

Holm, in the 1930s, presented a theory for calculating the contact resistance of a single contact spot. His model did not consider the influence of film and multi-spot contact on contact resistance [5]. Using Holm analysis, contact resistance for one circular contact spot is given by:

$$Rc = \frac{\rho}{2a} \tag{1}$$

where: ρ – the resistivity of the conductor and a – radius of the constriction.
For cases where the bodies in contact differ in material properties i.e., having different resistivity ρ_1 and ρ_2, the constriction resistance becomes:

$$Rc = \frac{\rho_1 + \rho_2}{4a}. \tag{2}$$

In 1966, Greenwood made a broader interpretation of Holm's model and presented a model for calculating contact resistance considering multi-spot contact. His model also did not consider the influence of surface film [6]. The contact resistance using Greenwood's analysis for multiple spots within a single cluster is given by the expression:

$$R_G = \frac{\rho}{2\sum a_i} + \frac{\rho}{\pi}\left(\sum_{i \neq j} \frac{a_i a_j}{s_{ij}}\right) \Big/ \left(\sum a_i\right)^2 \tag{3}$$

where ρ is the resistivity, s_{ij} is the distance between the centers of spots i and j; and a_i and a_j are the radii of spots i and j.

The first term $\frac{\rho}{2\sum a_i}$ represents the resistance of all the spots in parallel. The second term $\frac{\rho}{\pi}\left(\sum_{i \neq j} \frac{a_i a_j}{s_{ij}}\right) \Big/ \left(\sum a_i\right)$; represents the resistance due to the interaction between all the spots.

Greenwood made a further approximation of equation (3). When there is no correlation between the size of a given contact spot and its position, equation (3) becomes:

$$R_{G1} = \frac{\rho}{2\sum a_i} + \frac{\rho}{\pi n^2} \sum_{i \neq j} \frac{1}{s_{ij}}. \tag{4}$$

L. Boyer generalized Greenwood's formula, including surface film's influence on contact resistance [7]. Nakamura et. al also presented models for the calculation of contact resistance of contact spots (*a*-spots) with different shapes (square, hexagonal, triangular, etc.) [8].

This work aims to numerically analyze the thermal variation of a simplified contact model by comparing different scenarios of material properties of the contact spots using the finite element method (FEM) in COMSOL Multiphysics.

2. NUMERICAL MODEL DEVELOPMENT

The investigated problem is that of a simple metallic disc (copper) in contact via multiple contact spots (Fig. 2). Contact terminals inject a low DC of density j, and the distribution of the electric field is calculated using the finite element method (FEM) and COMSOL Multiphysics software.

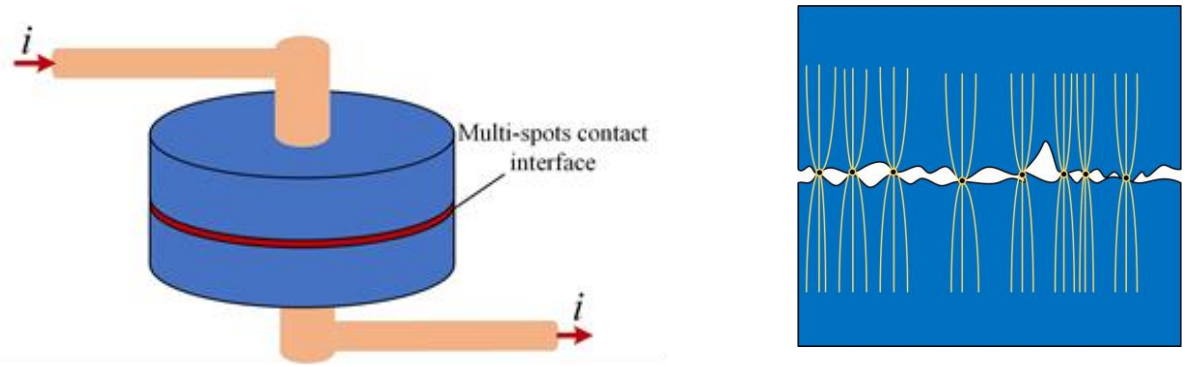

a) b)

Fig. 2 – (a) schematic view of the metallic disc, (b) constriction of current lines flowing through the contact spots

2.1 *Geometrical model*

The analysis investigates the contact of two metallic disks through multiple spots (a total of 28 identical circular contact spots) with the apparent area of contact having a thin insulating layer of polyethylene with high resistivity (Fig. 3). Both metallic discs have the following dimensions: radius α = 5 mm and thickness h = 1 mm. The contact spots each have a radius a = 0.1 mm. The insulating layer has a thickness of 30 μm.

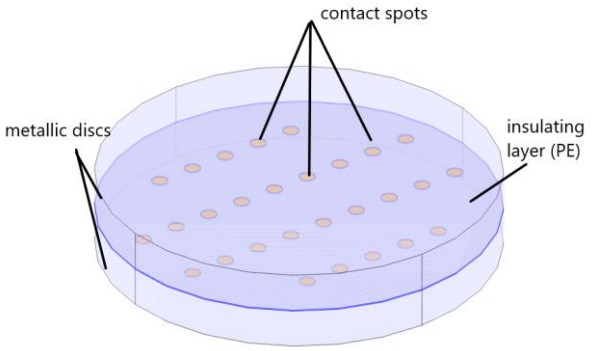

Fig. 3 – Geometric model showing the contact spots [9]

2.2. *Mathematical model*

The numerical analysis in this study consists of electromagnetic (electrical) and thermal problems.

Electrical problem: the electrical problem is in a stationary electro-kinetic regime with an imposed constant electric current of density $\boldsymbol{j}$ passing through the multiple contact spots. The fundamental equations governing the problem are the electric charge conservation law (6), the electromagnetic induction law (7), and the electric conduction law (8)

$$\operatorname{div} J = 0, \quad (6)$$

$$\operatorname{rot} E = 0, \quad (7)$$

$$J = \sigma \cdot E, \quad (8)$$

where σ[S/m] is the electric conductivity and E [V/m] is the electric field strength. E can be evaluated as a function of electric potential V as

$$E = -\operatorname{grad} V, \quad (9)$$

The boundary conditions are:

- Continuity $n \cdot (J_1 - J_2) = 0$. It specifies that the normal components of the electric currents are continuous across the interior boundaries of both metallic discs.

- Electric insulation $n \cdot J = 0$. It is applied on all surfaces except the contact spots; it specifies that no current flows across the boundaries.

Joule losses (volume density of electrical losses) are evaluated because the current flows from one medium of the copper disk through the contact spots to the other medium of the copper disk. It is calculated using the law of energy transformation.

$$P = J \cdot E = \sigma E^2. \quad (10)$$

Thermal problem: The thermal problem deals with the heat from the metallic disk due to resistive losses. The simplified contact model is placed in a box filled with air. The boundary condition is set at ambient temperature T_0 and is governed by the equation:

$$Q = \rho C_p \cdot dT/dt + \nabla \Psi, \quad (11)$$

where Q represents the heat source, and it is equivalent to the volume density of electrical losses. ρ [kg/m^3] represents density, C_p [J/(kg·K)] represents the specific heat capacity, and Ψ [W/m^2] represents the heat flux which is given by Fourier law;

$$\Psi = -\lambda \cdot \nabla T, \quad (12)$$

λ [W/(m·K)] represents the thermal conductivity which is considered constant (does not vary with temperature). The continuity equation is given by;

$$n \cdot (\lambda_j \cdot \nabla T - \lambda_k \cdot \nabla T) = 0. \quad (13)$$

The equations system (6)-(13) was solved using COMSOL Multiphysics and the finite element method. Figure 4 shows the discretization of the computational domain [9].

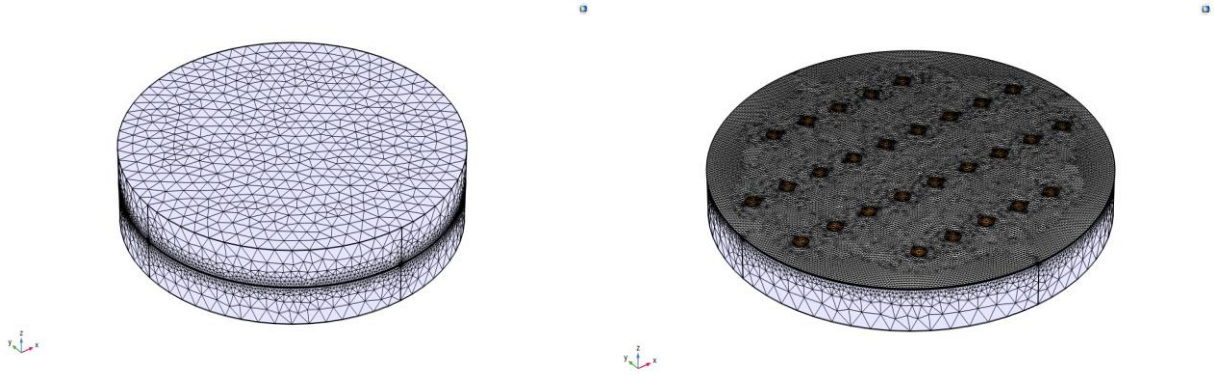

Fig. 4 – Discretization of the computational domain showing the contact spots

3. **RESULTS AND DISCUSSIONS**

Figure 5 shows the computed current flow lines for an applied current of 200 mA (J = 2.546·10^{-3} A/mm^2).

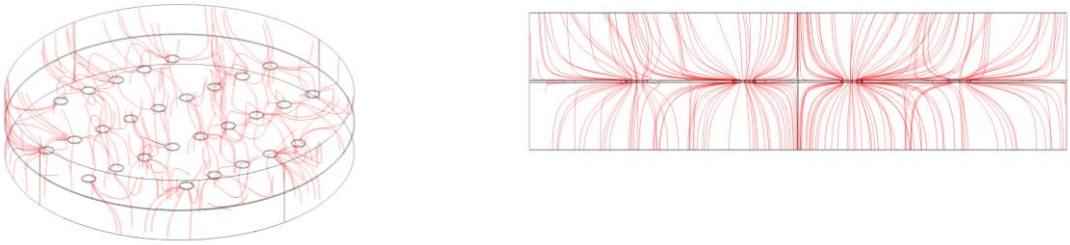

Fig. 5 – Constriction of current lines at the contact spots

Figure 6 shows a graphical representation of the calculated contact resistance values for both Holm's (1) and Greenwood's (4) equations, and the value computed numerically. The contact resistance decreases as the contact spot radius increases in all three cases. The results show that when the contact spot radius increases from 0.1 mm to 0.3 mm, the contact resistance decreases from $3.07 \cdot 10^{-6}$ Ω to $1.02 \cdot 10^{-6}$ Ω (Holm), $4.76 \cdot 10^{-6}$ Ω to $2.71 \cdot 10^{-6}$ Ω (Greenwood) and $3.25 \cdot 10^{-6}$ Ω to $4.34 \cdot 10^{-7}$ Ω (numerical simulation). And when the contact radius increases to 0.5 mm, the contact resistance becomes $6.14 \cdot 10^{-7}$ Ω (Holm), $2.30 \cdot 10^{-6}$ Ω (Greenwood), and $3.47 \cdot 10^{-7}$ Ω (numerical simulation) [9].

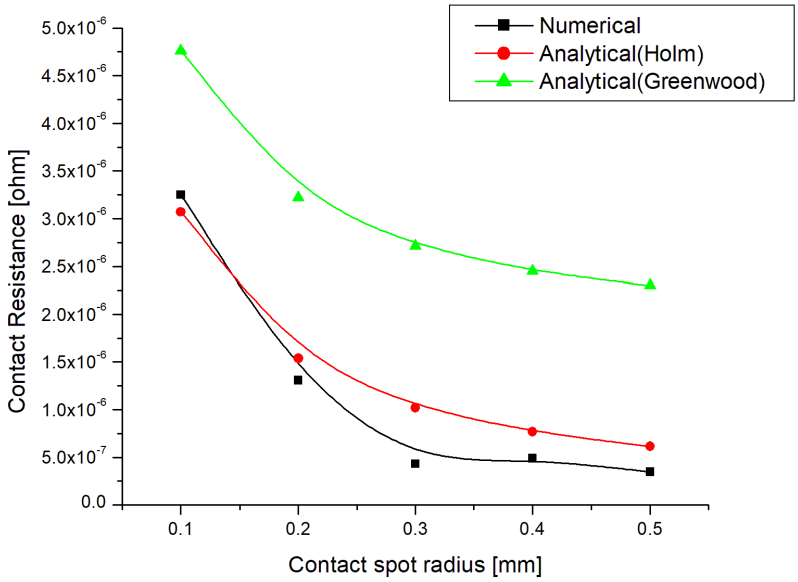

Fig. 6 – Contact resistance calculation showing analytical values Holm (1) and Greenwood (4) and numerical simulation values [9]

2.2. *Thermal analysis of the contact model*

The thermal analysis presented in this study will be for the numerically computed contact resistance from Fig. 6 because both Holm and Greenwood models are analytical models, and it won't be very easy to do a thermal analysis.

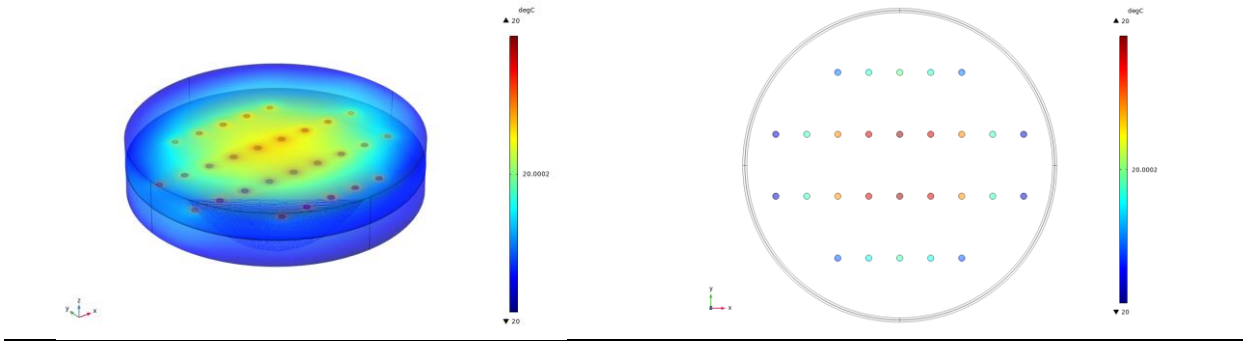

a)

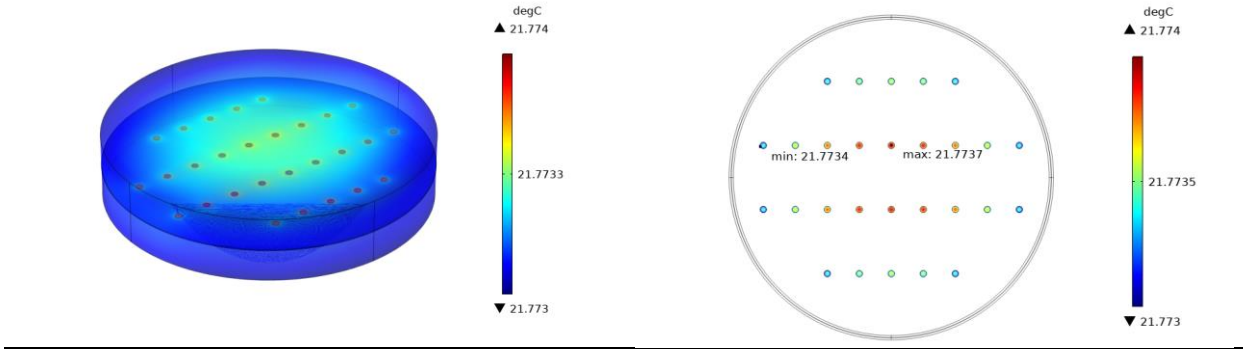

b)

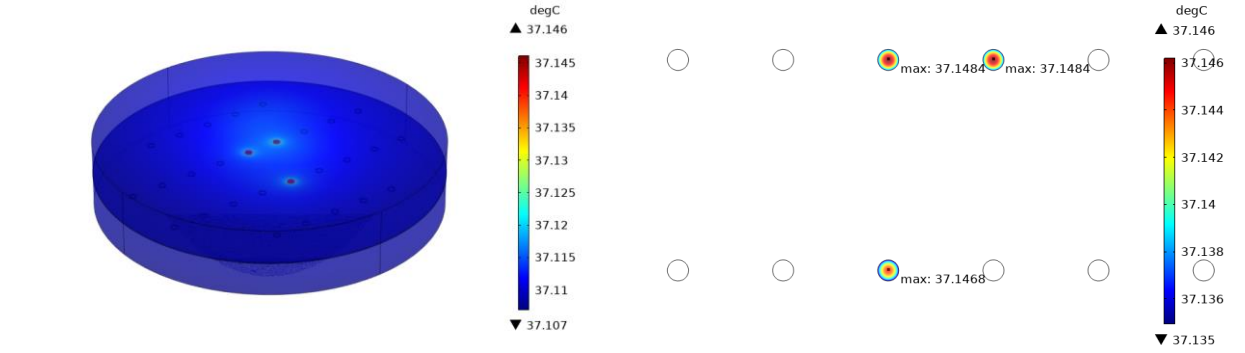

c)

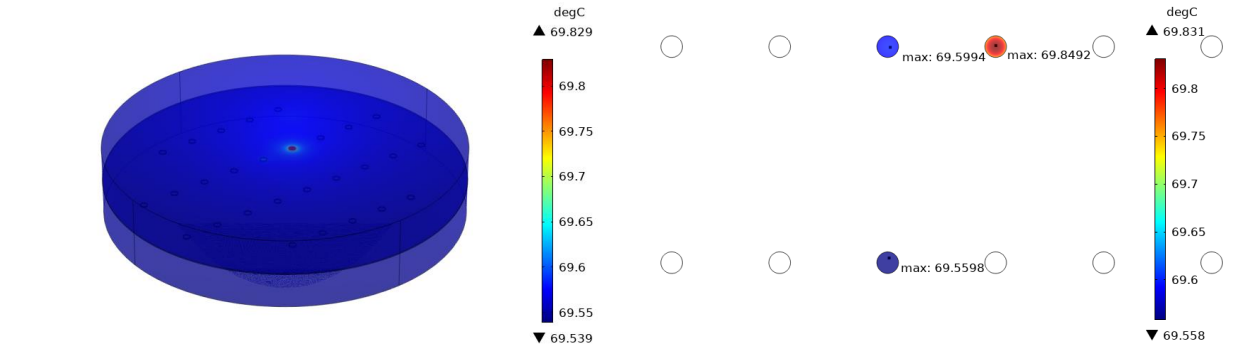

d)

Fig. 7 – Temperature distribution *a*) 28 contact spots ($\rho_{Cu\text{-}disk} = \rho_{Cu\text{-}spots} = 1.72 \cdot 10^{-8}$ Ωm); *b*) 28 contact spots ($\rho_{Cu\text{-}spots} = 1 \cdot 10^{-3}$ Ωm, $\rho_{Cu\text{-}disk} = 1.72 \cdot 10^{-8}$ Ωm); *c*) 3 contact spots ($\rho_{Cu\text{-}spots} = 1 \cdot 10^{-3}$ Ωm, $\rho_{Cu\text{-}disk} = 1.72 \cdot 10^{-8}$ Ωm); *d*) 3 contact spots ($\rho_{Cu\text{-}spots1} = 1 \cdot 10^{-3}$ Ωm, $\rho_{Cu\text{-}spots2} = 1 \cdot 10^{-2}$ Ωm, $\rho_{Cu\text{-}spots3} = 1 \cdot 10^{-1}$ Ωm, $\rho_{Cu\text{-}disk} = 1.72 \cdot 10^{-8}$ Ωm).

Figure 7 shows the steady-state temperature distribution of the contact model for an injected current of 200 mA ($2.546 \cdot 10^{-3}$ A/mm^2), $\rho_{Cu\text{-}disc} = 1.72 \cdot 10^{-8}$ Ωm, $\rho_{PE} = 1 \cdot 10^{17}$ Ωm, T_0 = 20 °C, a = 0.1 mm and 28 contact spots with $\rho_{Cu\text{-}spots} = 1.72 \cdot 10^{-8}$ Ωm (*a*), 28 contact spots with $\rho_{Cu\text{-}spots} = 1 \cdot 10^{-3}$ Ωm (*b*), 3 contact spots with $\rho_{Cu\text{-}spots} = 1 \cdot 10^{-3}$ Ωm (*c*), 3 contact spots having resistivity ($1 \cdot 10^{-3}$ Ωm, $1 \cdot 10^{-2}$ Ωm, and $1 \cdot 10^{-1}$ Ωm respectively) (*d*).

Figure (7a) shows no significant rise in temperature. The maximum temperatures in Fig. 7 (*b*), (*c*), and (*d*) are 21.77 °C, 37.14 °C, and 69.83 °C respectively which indicates that with the decrease of conducting spots of the contact, the temperature shows an increasing trend. Wang Shujuan et.al [1] presented a simulation of contact temperature rise based on a rough surface contact model. His results indicated that an increase in the contact area can effectively decrease contact temperature rise to some extent and vice versa. The computational result also shows that high-temperature concentration exists at the contact spots located at the core of the contact model.

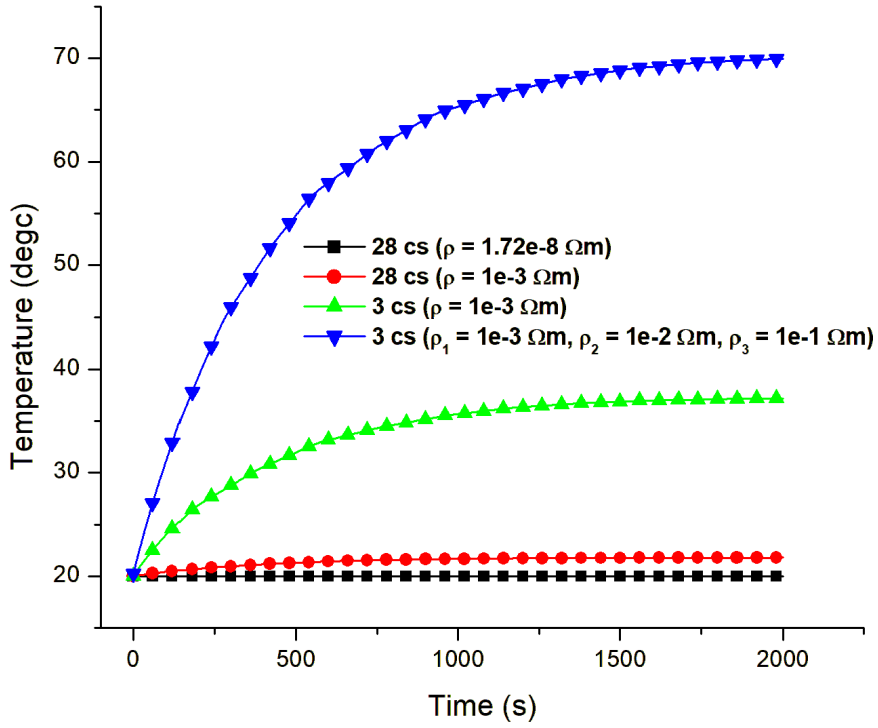

Fig. 8 – Temperature variation with time obtained for all four cases

Figure 8 shows the temperature variation of the four case studies presented in Fig. 7. The result clearly shows that when all 28 contact spots are operating under normal conditions with a resistivity of $\rho_{Cu\text{-}spots} = 1.72 \cdot 10^{-8}$ Ωm (■), there is no significant rise in temperature. In a case where all 28 contact spots have a resistivity of $\rho_{Cu\text{-}spots} = 1 \cdot 10^{-3}$ Ωm (●), the temperature increases to 21.77 °C. In general, such a temperature value does not affect the operation of the contact for short periods (of the order of hours). However, combined with other possible external factors mentioned above, the temperature can accelerate the degradation processes of the metal contact and its hosting.

In the worst-case scenario, where maybe due to electro erosion, aging of the contact, long-term accumulation of insulating oxide films at the contact zone, etc. only 3 contact spots are still conducting with a resistivity of $\rho_{Cu\text{-}spots} = 1 \cdot 10^{-3}$ Ωm (▲), there is a very significant rise in temperature to 37.14 °C, and when the 3 contact spots have resistivities of $\rho_{Cu\text{-}spots1}$ =

$1 \cdot 10^{-3}$ Ωm, $\rho_{Cu\text{-}spots2} = 1 \cdot 10^{-2}$ Ωm, and $\rho_{Cu\text{-}spots3} = 1 \cdot 10^{-1}$ Ωm respectively (▼), the temperature becomes 69.83 ^{o}C. In practice, it is typical of degraded electrical contact where on one hand, some spots at the interface possess high resistivity (contact resistance) due to a large accumulation of impurities and thus, have high-temperature concentration. On the other hand, spots with few or no impurities possess low resistivity. This possible high-temperature value leads in a very short time to total damage of the contact and all the consequences for the whole electrical circuit. This is consistent with the works of Shibata et.al [10], who performed some analysis of the contact distribution of fretting corrosion on samples made up of phosphorus-bronze alloy covered with tin plating. His analysis indicated that the parts with few oxide deposit layers possessed low contact resistance, while the parts with large oxide deposit layers possessed high contact resistance. Swingler et.al [11] studied the degradation of road-tested automotive connectors. He reported that high temperatures promote both physical and chemical processes leading to the degradation of connectors.

4. **CONCLUSION**

The present paper presents a thermal analysis of an electrical contact model of two metallic copper disks interacting through 28 homogenous circular spots of radius 0.1 mm. The study was done while keeping the resistivity of the copper disks constant and changing the resistivity of the contact spots as a possible ramification of degraded contacts. Figure 6 presents the calculation of contact resistance using two analytical models (Holm and Greenwood) and a numerical model in COMSOL Multiphysics. The thermal analysis presented in this paper correlates with only the numerical model for contact resistance calculation. As expected, the resulting temperature values indicate that the temperature increases as the resistivity of the contact spots increases and the functional contact area decrease. On a microscale level, in degraded electrical contact where only a small part of the interface is conducting, the high-temperature concentration coupled with other degrading factors accelerates the aging of the contacts. It promotes the movement of materials (electro-erosion), eventually leading to the failure of electrical contacts.

ACKNOWLEDGEMENT

The work was presented at the Symposium of Electric Machines SME'XVIII, in 2022.

REFERENCES

1. Wang Shujuan, Hu Fang, Su Bonan, Zhai Guofu, *Method for calculation of contact resistance and finite element simulation of contact temperature rise based on rough surface contact model*, 26th International Conference on Electrical Contacts, pp. 317-321, 2012.
2. R.S. Timsit, *Electrical contact resistance: properties of stationary interfaces*, IEEE Transactions on Components and Packaging Technologies, **22**, *1*, pp. 85-98, 1999.
3. Y. Fukuyama, N. Sakamoto, N. -h. Kaneko, T. Kondo, M. Onuma, *Constriction resistance of physical simulated electrical contacts with nanofabrication*, IEEE 60th Holm Conference on Electrical Contacts, pp. 1-5, 2014.
4. G.G. Dankat, A.A. Dobre, L.M. Dumitran, *Influence of ageing on electrothermal condition of low current contact*, 12th International Symposium on Advanced Topics in Electrical Engineering (ATEE), pp. 1-6, 2021.
5. R. Holm, *Electric contacts, theory and application*, Berlin: Springer-Verlag, 4th Edition, 1967.
6. J.A. Greenwood, *Constriction resistance and the real area of contact, Brit. J. Appl. Phys.*, **17**, pp. 1621–1632, 1966.
7. L. Boyer, *Contact resistance calculations: generalizations of Greenwood's formula including interface films*, IEEE Transactions on Components and Packaging Technologies, **24**, *1*, pp. 50-58, 2001.
8. M. Nakamura, *Computer simulation for the constriction resistance depending on the form of conducting spots*, IEEE Transactions on Components, Packaging and Manufacturing Technology Key Factor Analysis, **18**, pp. 382–383, 1995.

9. G.G. Dankat, A.A. Dobre, L.M. Dumitran, *Calculul analitic și numeric al rezistenței electrice într-un contact metalic, multi-punct, pentru curenți slabi*, APME, **17**, *1*, pp. 52–59, 2022.
10. Y. Shibata et al., *Detailed analysis of contact resistance of fretting corrosion track for the tin-plated contacts*, 26th International Conference on Electrical Contacts (ICEC 2012), pp. 228-232, 2012.
11. J. Swingler, J.W. McBride, C. Maul, *The degradation of road-tested automotive connectors*, IEEE Transaction on Components and Packaging Technologies, **23**, *1*, pp. 157–164, 2000.